Etching of Surfactant from Solution-Processed, Type-Separated Carbon Nanotubes and Impact on Device Behavior

Alexander A. Kane, Alexandra C. Ford, April Nissen, Karen L. Krafcik, and François Léonard*

Sandia National Laboratories, Livermore, California 94551, United States

ABSTRACT Semiconducting single-walled carbon nanotubes (SWCNTs) have great potential for use in electronic and optoelectronic devices. However, methods for synthesizing SWCNTs produce a mixture of metallic and semiconducting materials, which require additional processing to separate by electronic type. Purification and enrichment of the semiconducting fraction is readily achieved by using the centrifugation of aqueous suspensions of SWCNTs with the help of surfactants, but this leaves residual surfactant on the SWCNT surface that can impact their electronic and optical properties. Here, we present a detailed study of the sodium taurodeoxycholate (STDC) surfactant removal process during vacuum annealing, showing that it occurs through fragmentation of the surfactant, and that complete removal requires exceedingly high temperatures, which indicates strong binding to the SWCNTs. We then present an approach based on air oxidation and mild annealing to completely remove the surfactant while maintaining the SWCNT properties. Using this approach, we compare single SWCNT electronic devices with and without STDC and show that, despite the very strong surfactant binding, it does not affect device performance substantially.

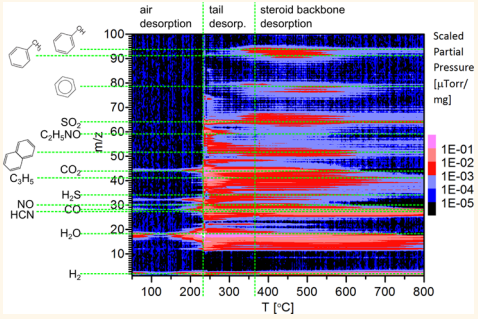

KEYWORDS: carbon nanotubes · transistors · functionalization · surfactant · air oxidation · purification

Single-walled carbon nanotubes (SWCNTs) have the potential to be a cornerstone material for emerging electronic and optoelectronic nanotechnologies, with demonstrated applications such as transistors for high-performance computing,[1] flexible and transparent electronics,[2] nanoscale light emission and detection,[3] and chemical sensing.[4,5] For these applications, semiconducting SWCNTs are required, but existing growth processes yield a mixture of semiconducting and metallic SWCNTs. One of the most promising methodologies to solve this problem is postgrowth solution-processing of SWCNTs, such as density-gradient ultracentrifugation (DGU),[6] gel chromatography,[7] and selective polymer wrapping.[8]

While these methods have demonstrated the separation of metallic and semiconducting SWCNTs, electronic devices fabricated from such SWCNTs are much more resistive than state-of-the-art devices fabricated directly from CVD-grown SWCNTs.[7−13] An open question is what role surfactants and other molecules introduced during the solution processing play in this degradation of device properties. For example, residual surfactant along the SWCNT channel may cause scattering, decreasing mobility in FETs.[8,10,12,14−16] The residuals are certainly problematic for chemical sensors since residual surface molecules will alter the chemistry of the SWCNT sidewall, blocking access or otherwise mediating reactions.[17,18] For optoelectronics, adsorbed surfactant can impact exciton diffusion length,[19] broaden absorption peaks,[20] and lead to photoluminescence sidebands and blinking.[21] Previous studies have examined physical and chemical approaches to remove the surfactant, focusing mainly on films of SWCNTs. While these approaches have shown a general improvement in device cleanliness, their effectiveness in removing the surfactant from the SWCNTs themselves has not been established. The aforementioned studies do not usually present direct analysis of the surfactant removal process, and only one presents the impact on individual SWCNT-based device properties, with the

* Address correspondence to fleonar@sandia.gov.

Received for review November 25, 2013 and accepted February 10, 2014.

Published online February 10, 2014
10.1021/nn406065t

conclusion that removal of the surfactant improves device behavior.[15]

The physical processes used to remove surfactants include filtration,[9,22] rinsing and soaking in solvents,[15] and annealing in inert environments.[8,23] These methods are not general since the binding energies and density around the SWCNTs can vary widely across molecules[17] and polymers.[24] Filtration requires resuspension of the SWCNTs in dichloroethane using ultrasonication, which damages them.[25] Rinsing can remove the bulk of the surfactant but not the closest, strongly adhered layer to the SWCNT sidewall, as demonstrated by microscopy.[20] Soaking and rinsing approaches for surfactant removal may also lead to SWCNTs going into solution, thus reducing the SWCNT density or even redepositing them in unwanted locations. This can be avoided by pinning the SWCNTs down with metal contacts prior to the soaking process,[15] but then surfactant may also be pinned between the metal and SWCNT, potentially increasing contact resistance. Further, these processes target the surfactant but not other molecules introduced to aid deposition which can also affect device properties.[26]

Chemical approaches to remove the surfactant have focused on oxidation, including oxidation in nitric acid and heating in air. These take advantage of the greater oxidative reactivity of sp^3- over sp^2-hybridized carbon bonds and may therefore be more general to remove surfactants and other organic contaminants.[27] Oxidation in nitric acid has been shown to increase the conductivity of transparent conductive films of SWCNTs[16,20,28−30] and to be more effective than rinsing alone.[20] Unfortunately, the nitric acid damages the SWCNTs,[20,30] and much of the resistance decrease can be attributed to oxidative doping of the semiconducting SWCNTs to form more paths in the percolating networks.[29,30] O_2 oxidation through the laser heating of substrates in air can remove surfactant in dense networks,[31] but this process may be difficult to implement in a production setting as it uses a laser rastering process, and its efficacy on removing surfactant from the SWCNT sidewall was not evaluated directly.

Thermal treatments are an attractive alternative technique to remove surfactants, as this may also result in overall cleaner devices, and annealing is nearly universally used as a final step to clean solution-processed SWCNT devices.[7−9,11,15,30] However, the effectiveness of annealing at removing surfactant from encapsulated SWCNTs has not been directly evaluated. Instead, indirect measurements of SWCNT properties, such as photoluminescence, were used.[23]

In this article, we begin by examining the effectiveness of thermal techniques at removing sodium taurodeoxycholate (STDC) surfactant from SWCNTs through direct measurement. Using temperature-programmed desorption (TPD), we present a detailed study of the desorption of the STDC from SWCNTs during vacuum annealing, showing that it occurs through fragmentation and requires very high temperatures for complete removal, indicating strong binding to the SWCNTs. Next, we present and analyze a more effective and general procedure to etch the surfactant from SWCNTs on a wafer substrate using air oxidation. AFM analysis and Raman spectroscopy show that the etch incurs minimal damage to the SWCNTs, and the adsorbed oxygen from the procedure can be removed using a low-temperature vacuum anneal. Application of the process is illustrated through the fabrication of field-effect transistors with individual SWCNTs, and comparison of devices with and without the surfactant shows that STDC dopes the SWCNTs but does not substantially impact the field-effect mobility.

RESULTS AND DISCUSSION

Analysis of Surfactant Desorption in Vacuum. We began by analyzing surfactant desorption from SWCNTs during annealing in vacuum in order to assess the effectiveness of this approach and the strength of the surfactant binding. SWCNT material with the STDC surfactant was prepared as described in the Methods section and subjected to mass spectroscopy (MS) temperature-programmed desorption. Figure 1 plots the evolution of the gases as the SWCNT sample was heated in UHV. The figure shows that a broad range of molecular species evolves, with some species observed at temperatures as high as 800 °C. At 230 °C, most of the water was removed and the STDC surfactant began to pyrolyze, with the aliphatic tail coming off between 230 and 370 °C. This is revealed by the presence of sulfur- (H_2S and SO_2) and nitrogen-containing gases (NO and acetamide) with peaks seen at principal mass to charge ratios m/z = 32, 64, 30, and 59, respectively. The remaining steroid groups were mostly removed over a broad range of temperatures from 450 to 650 °C, as seen by the clusters of peaks near m/z = 51, 64, 78, and 94.

Although the principal peaks of the whole steroid groups are above the range of the residual gas analyzer and could not be detected, these fragmentation patterns suggest that the groups were fragmented and aromatized before desorption, as each cluster of peaks had different temperature dependences, and the clusters are centered around m/z numbers characteristic of aromatic hydrocarbons such as benzene, benzene derivatives like toluene and phenol, and naphthalene. The desorption of some of these molecules continued to very high temperatures, with species still detected above 800 °C, such as the line at m/z = 64 (see also Supporting Information Figure S3). This fragment likely corresponds to naphthenic hydrocarbons, further confirmation that these groups have stronger interactions the SWCNTs than with benzene groups.[32] These studies show that, at least for STDC, vacuum annealing alone is an inefficient process for surfactant removal

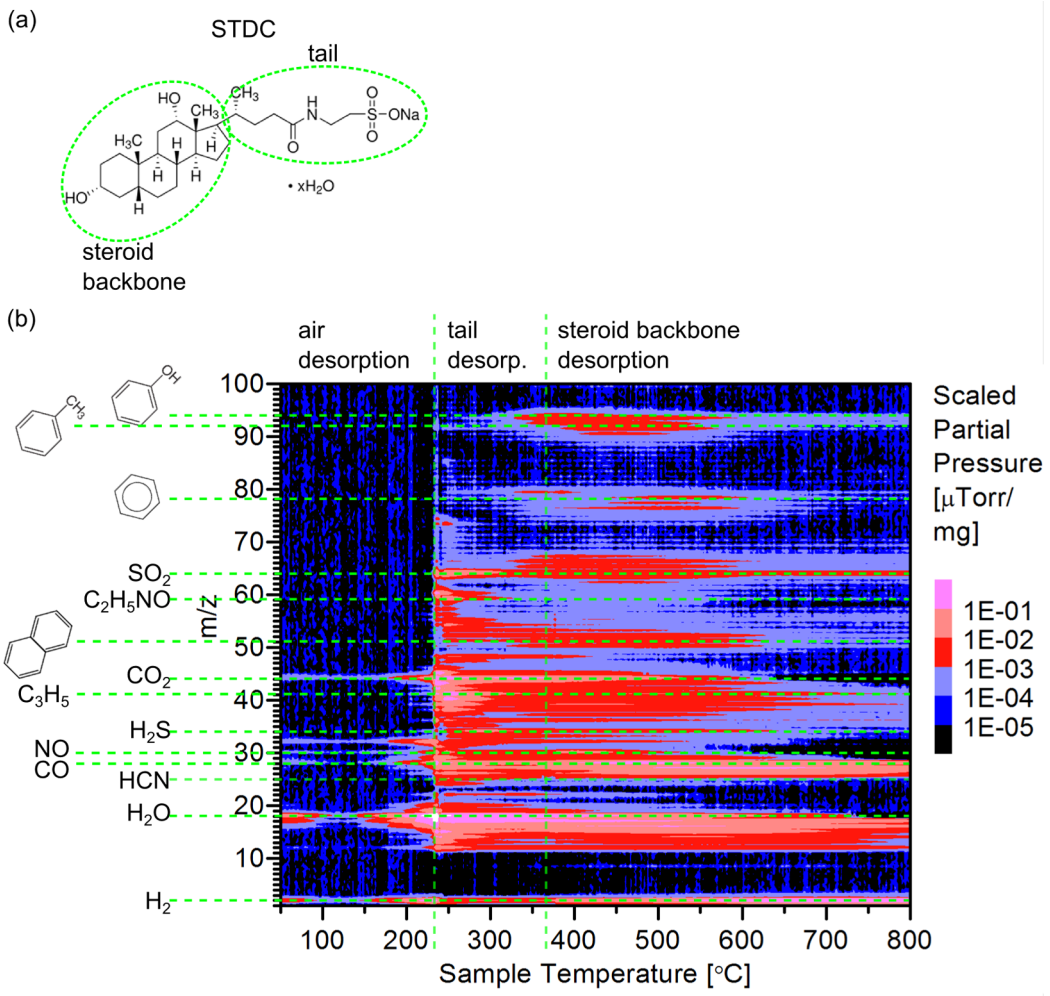

Figure 1. (a) Structure of the STDC surfactant.[33] (b) Results of temperature-programmed desorption of the surfactant and adducts from the ultracentrifuged SWCNTs. The horizontal dashed lines point to the molecular species that are evolving, while the vertical dashed lines denote the temperature regions where desorption of the tail and steroid groups from the surfactant are observed. For each species identified, only the *m/z* ratio of the principal peak is labeled, but for identification, the full MS fingerprint was used. Expanded data can also be found in Figure S3.

and requires temperatures that are too high for many fabrication processes. We expect that other processes which also rely on thermal desorption of the surfactant in vacuum (*e.g.*, laser or joule heating) would suffer from the same issues.

Oxidative Process for Surfactant Removal. In order to get around the issues with the purely physical thermal desorption process, we developed a chemical process based on mild oxidation in air. The goal (and challenge) of this etching process is to remove the surfactant functional groups without impacting the SWCNTs. We thus began by performing thermogravimetric analysis (TGA) in dilute air (Methods) to investigate whether any region could be identified where the surfactant and SWCNT oxidative burning could be decoupled. Figure 2a shows TGA curves for the SWCNT material as-purchased (AP), the suspended SWCNT material after the first sonication in surfactant solution (FS), and the SWCNT material after the first ultracentrifugation step (UC) (see Methods). The AP and FS samples contained substantial amounts of catalyst, whereas the UC sample contained less than 1% by weight, as measured by the remaining mass[34] after oxidation at 1000 °C. As a consequence, the SWCNTs burn primarily between 550 and 850 °C in the UC sample but are completely combusted by 600 °C in the FS sample, because of the high concentration of active catalyst. The SWCNTs burn at an intermediate temperature range in the AP sample, between 500 and 800 °C, because catalyst particles are present but are deactivated until the carbon shells surrounding them are removed.[35] As a consequence of the temperature ranges for SWCNT combustion in the FS sample, it is difficult to identify a region where the surfactant can be oxidized without burning the CNTs. However, the differential TGA curves of Figure 2a show that the UC material has a clear separation between the surfactant and SWCNT combustion regions, allowing for selective etching of the surfactant. The mass loss seen above 900 °C, largest in the FS sample, likely results from the oxidation of other non-SWCNT

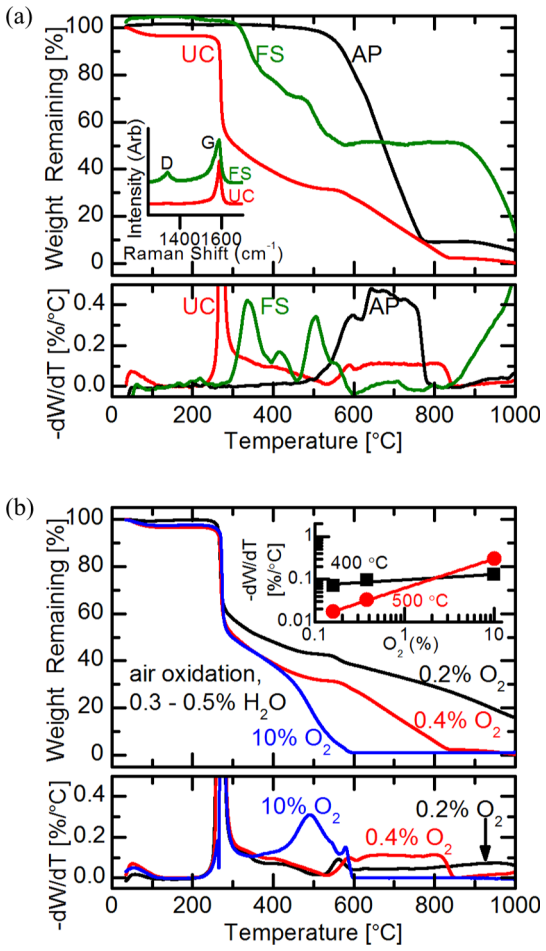

Figure 2. (a) TGA curves showing percentage of weight remaining and corresponding derivative weight loss, as a function of temperature in air (0.4% O_2, 0.3% H_2O) for the as-purchased (AP) CNT material, suspended CNT material after first sonication in liquid (FS), and CNT material after low-power ultracentrifugation (UC). The Raman spectra in the inset show the absence of the carbonaceous species in the UC material as evidenced by the reduction of the D peak. (b) TGA curves for the ultracentrifugated SWCNT material for three different oxygen concentrations and the corresponding derivative weight loss. The inset shows the derivative weight loss rate for two temperatures as a function of oxygen concentration.

graphitic carbons. These are largely removed by ultracentrifugation, explaining their relative absence in the UC material.

The selectivity of the process is dependent on the oxygen concentration, as seen from TGA data of the UC material taken at different oxygen concentrations at atmospheric pressure (Figure 2b). The SWCNT burn rate remains low at temperatures below 520 °C for oxygen concentrations of 0.38% or lower, but at a concentration of 10%, the surfactant burning region and the SWCNT burning region overlap. This oxygen concentration dependence is seen clearly in the inset of Figure 2b, in which the total burn rates at 400 °C, where the mass loss is due mainly to the combustion of surfactant, and at 500 °C, where the mass loss is due primarily to the combustion of SWCNTs, are plotted.

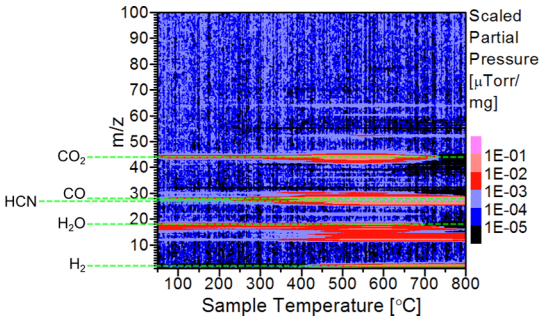

Figure 3. Results of temperature-programmed desorption of the surfactant and adducts from the ultracentrifuged SWCNTs after oxidation. The horizontal dashed lines point to the molecular species that are evolving. For each species identified, only the *m/z* ratio of the principal peak is labeled, but for identification, the full MS fingerprint was used. Expanded data can also be found in Figure S4.

Over these partial pressures, the surfactant combustion has little dependence on the oxygen concentration compared to the SWCNTs, so that a window for preferential etching of the surfactant exists at small oxygen concentrations.

Water, another reactive component of air, was also present during the TGA experiments, with concentrations ranging from 0.3 to 0.5%. Even though water was not consumed during the oxidation of the surfactant or the SWCNTs (see Figure S5), water could still have been catalytically active in the oxidation. Further experiments involving oxidation in dry O_2 and pure H_2O are necessary to clarify the roles of water and oxygen in the oxidation processes.

We characterized the effectiveness of the oxidation process at removing the surfactant by again performing MS TPD analysis. The SWCNT sample was first heated in a furnace at 500 °C in air for 10 min. As shown in Figure 3, upon heating the oxidized sample in UHV, little trace of surfactant-related species was detected. In comparison with Figure 1, Figure 3 is very sparse, with the only faint surfactant-related peaks detected above the background occurring at 560 °C for m/z = 52, 60, and 64. Figure 3 also lacks the characteristic multipeak patterns that are seen when multi-carbon organics are present, as in Figure 1. The faint residuals may result from incomplete oxidation of the surfactant or products from the oxidation that are adsorbed on the porous alumina crucible.

While the oxidation process was effective at removing the surfactant, Figure 3 also shows that significant peaks appear at mass ratios of 28 and 44, which can be attributed to CO and CO_2. These are due to the adsorption of oxygen on the SWCNTs during the etch process, with broad desorption peaks indicative of the variety of absorption environments present within the sample. The relatively low peak desorption temperatures (605 and 534 °C) suggest that the majority of the oxygen is either physisorbed or chemisorbed as carboxyl groups.[36,37] The chemisorbed O_2, which desorbs

mainly as CO, may replace H groups on the ends of the SWCNTs or at pre-existing defect sites, as the increase in the amount of CO desorbed near 600 °C in the oxidized sample is accompanied by a 1:1 decrease in the amount of H_2 desorbed near 750 °C when compared to the unoxidized sample (see Figure S4 for expanded data).

Etching Surfactant from SWCNTs on Si Wafers. The oxidation process was further tested on SWCNT material deposited on Si wafers (see Methods). AFM and Raman spectroscopy were used to examine the chemical and structural changes in the SWCNTs due to the etching and annealing processes. AFM analysis[38] of SWCNTs dispersed on substrates confirms that the etch selectively removes the surfactant, leaving the SWCNTs morphologically unchanged. Qualitatively, the SWCNTs were more clearly resolved in the etched samples, because of the removal of the surfactant and aminopropyltriethoxysilane (APTES), (Figure 4a,b). The aerial density (~50 SWCNTs/100 μm^2) was unchanged after etching at 300, 400, and 500 °C for 10 min. After a 600 °C oxidative etch, all of the SWCNTs were removed. Figure 4c shows the corresponding length distributions of the identically prepared samples as a function of etching temperature. No significant changes were seen in the distributions or mean SWCNT lengths between samples. Experiments with SWCNTs purchased from NanoIntegris, Inc. also showed no changes in those parameters postetch, suggesting that the etch should be broadly applicable for catalyst-free SWCNT preparations.

To further characterize the effects of the etch process and surfactant removal on the SWCNTs, and the reversibility of the oxygen adsorption, Raman spectra were taken on SWCNT samples at different stages of the standard etch recipe (500 °C oxidation in air, 600 °C anneal in high vacuum) and on samples etched with other etch recipes for comparison (See Supporting Information Figure S6). The effects of the fragmentation and the removal of the surfactant, the O_2 absorption, and recovery of the pristine SWCNTs at different stages of the etch process can be seen in the Raman spectra in Figure 5a. These are normalized spectra without background subtraction, covering the RBM, D, G, and 2D peak regions. For the material as-deposited, all the significant peaks[39] were easily distinguishable from the flat background, as the surfactant did not strongly scatter the 532 nm light or quench the Raman signal from the SWCNTs. After etching at 380 °C, a broad photoluminescent (PL) background emerged and the signal from the SWCNTs was diminished. This PL background likely comes from partially oxidized and fragmented surfactant. The background was not present in the samples oxidized at 500 °C (*i.e.*, after removal of the surfactant), and the SWCNT peaks were again the most prominent features. In these, the RBM and D peaks were greatly diminished when compared to the initial spectra, but they were restored by annealing the samples at 600 °C in vacuum to remove the adsorbed oxides. The final spectrum was very similar to the starting one, indicating recovery of the material.

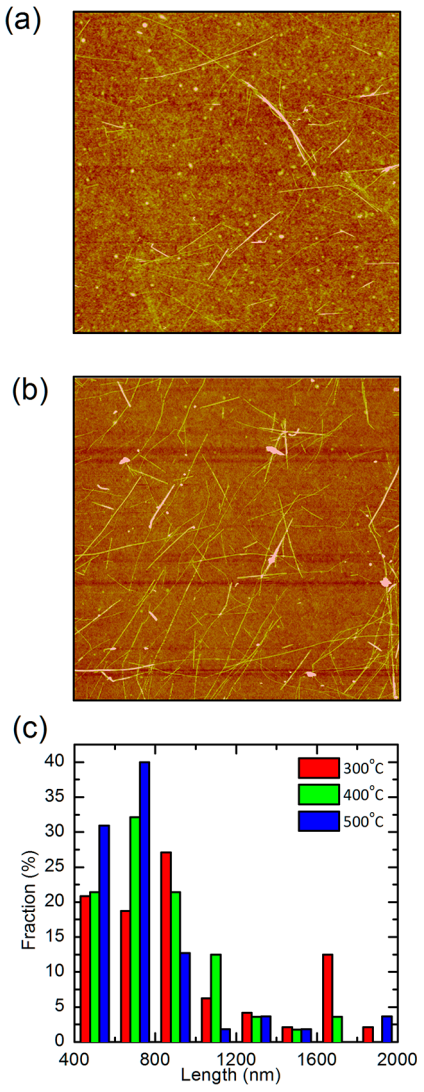

Figure 4. AFM height images (5 μm × 5 μm) of the SWCNT material after ultracentrifugation, spin-cast onto an APTES-coated SiO_2/Si wafer (a) as-deposited and (b) in a different region after oxidizing at 500 °C for 10 min. (c) Comparison of SWCNT length distributions after oxidation at three different temperatures for 10 min. (*z*-scale: 0−5 nm)

High-resolution, background-subtracted Raman spectra (Figure 5b) show that the SWCNTs are doped by both the surfactant and the oxidation but are nearly intrinsic after the anneal. This lack of doping in the annealed SWCNTs is indicated by the presence of the Breit−Wigner−Fano (BWF) shaped peak[39] in the G^- band around 1520 cm^{-1}, which indicates free carriers near the band crossing point in metallic SWCNTs, broadening the peak because of the Kohn anomaly. The absence of this peak in the pristine and oxidized samples indicates doping[40] by the surfactant in the former and by the adsorbed oxygen in the latter. There is also a 2 cm^{-1} softening of the G^+ band from the

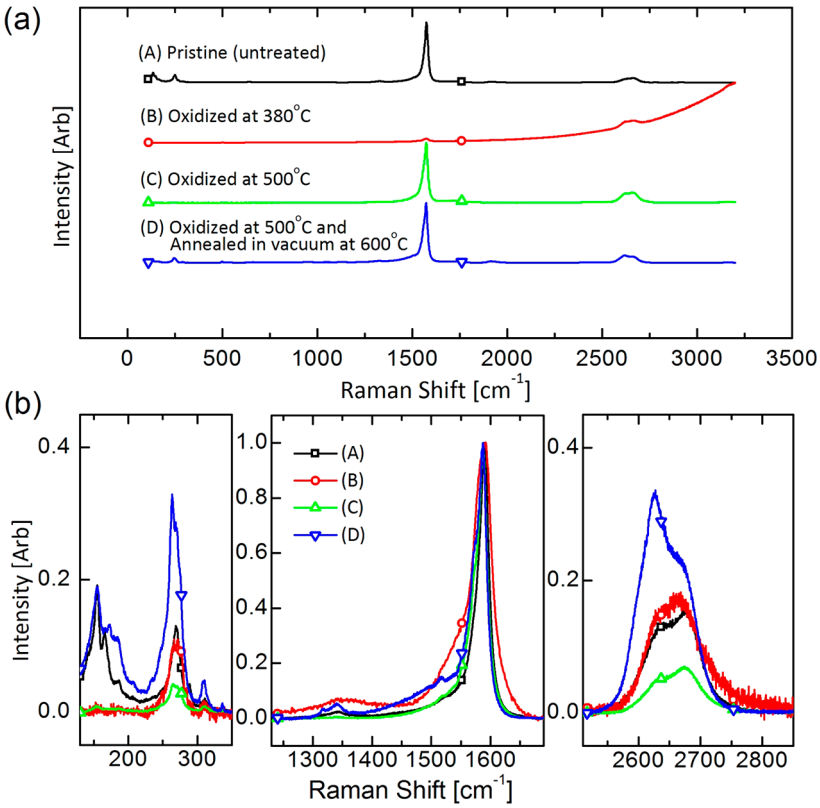

Figure 5. Raman spectra of SWCNT material after low-power ultracentrifugation, spin-cast onto an SiO_2/Si wafer, and thermally processed. (a) Composite Raman spectra over the entire region of interest without background subtraction, with traces offset for clarity. (b) (Left) Radial breathing mode region, (center) D and G peak region, (right) 2D peak region. The traces in (b) are normalized to the G peak near 1589 cm^{-1} after background subtraction.

pristine to the oxidized and annealed samples, indicating a doping[41] of about 1 hole/150 C atoms by the surfactant.

The strong doping due to the oxidation is evidenced by the quenching of the RBM, 2D, and D peaks after the oxidation.[41,42] The quenched peaks are completely restored upon annealing in high vacuum. There is a general enhancement of the signal for the etched smaller diameter SWCNTs (RBM peaks above 166 cm^{-1}, d < 1.5 nm) for the oxidized and annealed material when compared to the as-deposited material, possibly due to the removal of the surfactant, or other functional groups stemming from the purification process, that dope the more reactive smaller diameter SWCNTs. The quenching of the RBMs through oxidation is similar to that observed in recent work reporting type-specific oxidation.[43]

The ratio of the areas of the D and G peaks, A_D/A_G, is a measure of the concentration of disorder in the sample[44,45] and is also highly dependent on doping, varying by as much as 20% for small changes in carrier concentration and more for highly doped samples.[42] As discussed above, the SWCNTs start out doped by the surfactant and are p-doped during the etch, so quantitative comparison of the ratio at different etch steps is not meaningful. Qualitatively, however, the ratio is greatly increased by the fragmentation of the surfactant but otherwise is not changed by the etch process (Figure S7). This indicates that the surfactant does not serve as a significant source of disorder before etching, and that etching does not significantly increase the defect density in the SWCNTs.

Raman spectra taken on the bulk SWCNT samples used in the TPD and TGA experiments (see Figure S6) are very similar to the spectra taken for SWCNTs deposited on a wafer (Figure 5), confirming that the oxidation proceeds in a similar manner for both. These data also confirm that removing the surfactant by etching in air results in cleaner samples than simple annealing in UHV, as evidenced by the increased disorder (A_D/A_G) seen in the UHV annealed sample when compared to the data from the sample etched and annealed (see Figures S6 and S7).

Electronic Devices. As just discussed, one advantage of surfactant etching through mild oxidation is that it can be used as postprocessing, performed after the SWCNTs have already been deposited on substrates. This also allows for the comparison of electronic devices with and without the surfactant. Figure 6 shows the transfer characteristics for two representative single SWCNT devices fabricated using the semiconductor-enriched fraction of SWCNTs after density-gradient ultracentrifugation. The device in the main panel was fabricated (see Methods) using a SWCNT

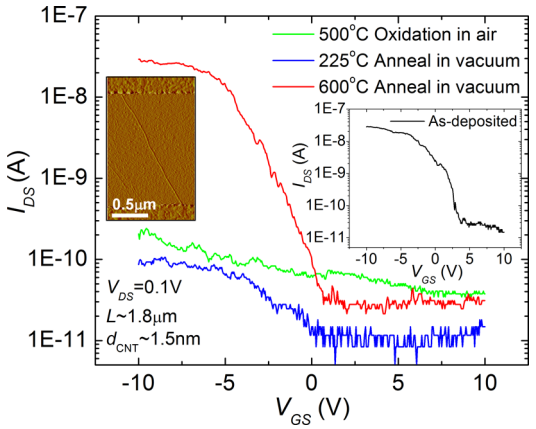

Figure 6. Transfer characteristics for a single SWCNT device fabricated using a SWCNT oxidized in air at 500 °C for 10 min, followed by annealing in vacuum at two different temperatures. The inset on the left shows an AFM image of the device. The inset on the right shows the transfer characteristic for a single-SWCNT device fabricated using an as-deposited (*i.e.*, unoxidized) SWCNT for direct comparison.

oxidized in air at 500 °C for 10 min, followed by first annealing in vacuum at 225 °C for 10 min and then annealing in vacuum again at 600 °C for 20 min. The device in the inset was fabricated using an as-deposited (*i.e.* unoxidized) SWCNT, followed by annealing in vacuum at 600 °C for 20 min, for direct comparison. Postoxidation, and prior to annealing, the oxidized SWCNT device exhibits very low ON current of ~0.2 nA and minimal gate dependence, due to the introduction of adducts during the oxidation. Following low-temperature annealing at 225 °C, the oxidized SWCNT device current remains low, indicating minimal recovery from the oxidation. However, after annealing at 600 °C, the oxidized SWCNT device has an ON current of ~30 nA and ON/OFF ratio >10^3, comparable to the behavior of the as-deposited device in the inset and our previously reported devices fabricated without oxidation,[46] as well as other as-deposited solution-processed SWCNT devices found in the literature. This recovery in device behavior suggests that most of the oxidation-induced defects have been removed by annealing at this temperature, in agreement with the Raman radial breathing mode spectra of Figure 5, and highlights the effectiveness of the oxidation and annealing process as a means to remove surfactant and adsorbates while minimizing the net introduction of defects.

To study the impact of the surfactant on device behavior, we fabricated a set of single SWCNT FETs with surfactant (*i.e.*, as-deposited) and another set without surfactant (*i.e.*, oxidized at 500 °C and annealed in vacuum at 600 °C). Figure 7a shows the distribution of threshold voltages for devices with and without the surfactant. The reduction in the threshold voltage upon surfactant removal is consistent with the Raman data, which indicates p-type doping of the SWCNTs by the surfactant. This threshold voltage shift of ~2 V corresponds to a doping on the order of

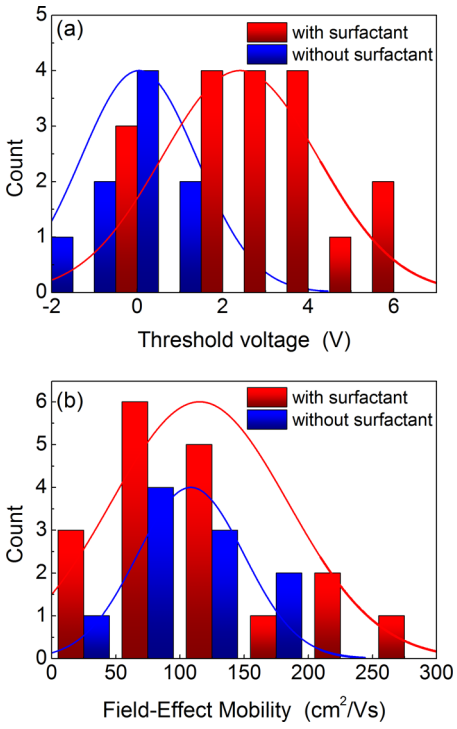

Figure 7. Impact of surfactant on SWCNT FETs. The distribution of (a) threshold voltages and (b) field-effect mobilities for devices with surfactant (as-deposited) and without surfactant (oxidized and annealed).

10^{-3} e/atom or 0.2 e/nm. Assuming a dense coverage of surfactant on the SWCNTs, this would correspond to a doping of roughly 1 e/molecule.

More importantly, we find that the surfactant has little impact on the field-effect mobility, as shown in Figure 7b. Indeed, for both sets of devices, we find average mobilities of ~120 cm^2/Vs. This value is a factor of 3 lower than the best reported field-effect mobilities for solution-processed SWCNT FETs of similar channel lengths,[9] most likely due to the quality of the as-purchased CVD-grown SWCNT material. Regardless, our work establishes that, for the range of SWCNT field-effect mobilities and channel lengths studied here, the surfactant does not appreciably degrade electronic transport in the channel.

CONCLUSION

In conclusion, we show that removing the surfactant from type-separated, solution-processed SWCNTs through vacuum annealing requires very high temperatures, with the removal dynamics occurring through fragmentation of the surfactant where the tail desorbs initially followed by the steroid group. A more effective approach for surfactant removal based on thermal oxidation is presented, which leads to complete removal of the surfactant. The method is shown to be applicable to on-substrate SWCNTs and their subsequent use in electronic devices, revealing doping of the SWCNT by the surfactant and no appreciable reduction of the field-effect mobility due to the

surfactant. This result can likely be extended to a range of surfactants, as other surfactants used for DGU are organic, with many of them being cholates very similar to STDC. More generally, the surfactant removal approach should be useful for sensing and optoelectronic devices based on carbon SWCNTs and should also be applicable to other nanomaterials where surfactants are used, such as graphene.

METHODS

Material Preparation. The commercially produced material (CVD-grown SWCNTs purchased from Cheap Tubes, Inc.) was suspended in a 1% STDC aqueous solution using ultrasonication. This solution was then centrifuged at low power (3 h at 12 000 rpm) to remove impurities. To sort the SWCNTs by electronic type, the top 2/3 of the centrifuged solution was then concentrated using a second ultracentrifugation step (18 h at 40 000 rpm), followed by density-gradient ultracentrifugation in an Optiprep density-gradient medium (18 h at 40 000 rpm). The as-purchased material is labeled AP, the suspended material after first sonication in liquid is labeled FS, and the material after the first ultracentrifugation step is labeled UC.

Samples were then prepared for thermogravimetric analysis, mass spectroscopy temperature-programmed desorption, and Raman spectroscopy by dropping close to 5 mg of concentrated suspension, prior to DGU, into alumina crucibles. These were baked at 200 °C for 5 min to remove excess water, leaving behind 0.3−2.9 mg of material. Samples for Raman spectroscopy were also prepared by dropping dilute material on a Si wafer for comparison with the material in the crucibles.

Thermogravimetric Analysis. TGA was performed in oxidizing conditions from room temperature to 1000 °C at a rate of 3 °C/min. Then, 1−20 mg of SWCNT suspensions was loaded into alumina crucibles and preheated to 270 or 380 °C for 10−20 min to evaporate most of the water, leaving 0.2 to 3 mg of residue. TGA was performed using a Mettler Toledo TGA/DSC 1 thermogravimetric analyzer. Air was used as the oxidizing gas with Ar used to dilute the oxygen concentration. The gas flow was maintained at 40 mL/min. Mass spectroscopy during the TGA experiment was performed with a Pfeiffer Vacuum ThermoStar GSD 301 T2 mass spectrometer.

Temperature-Programmed Desorption. TPD was performed in a vacuum furnace (base pressure $<5 \times 10^{-9}$ Torr) from room temperature to 1100 °C at a rate of ~3 °C/min. SWCNT suspensions were prepared as described in TGA methods above. Mass spectroscopy during the TPD experiment was performed with a Stanford Research System (SRS) 300 quadrupole residual gas analyzer.

Raman Spectroscopy. Samples were illuminated using a 532 nm YAG laser at a power of ~30 mW, focused with a 50× objective. The back-scattered light was collected, filtered with a Semrock edge filter, and dispersed onto a liquid-nitrogen-cooled CCD detector using 600 and 1800 groove/mm gratings.

Device Fabrication and Analysis. Back-gate field-effect transistor (FET) devices with channel lengths $L \sim 1-2\ \mu$m were fabricated to investigate electrical transport behavior as a function of oxidation and subsequent annealing. After density-gradient ultracentrifugation sorting, the primarily semiconducting SWCNTs were spin-cast at 2000 rpm onto 90 nm SiO_2/Si (p^+-doped) substrates that had been treated with APTES. Next (for the oxidized devices), the SWCNTs on SiO_2/Si substrates were oxidized in air at 500 °C for 10 min. Then photolithography was used to pattern the source and drain contacts, followed by e-beam evaporation of ~0.5 nm Ti/40 nm Pd and liftoff. Here the p^+ Si substrate serves as the global back-gate. Subsequent annealing steps at 225 °C for 10 min and 600 °C for 20 min were carried out in vacuum ($\sim 9 \times 10^{-6}$ Torr) for the oxidized devices. A single annealing step at 600 °C for 20 min was carried out in vacuum for the as-deposited devices. FET threshold voltages were obtained by averaging the threshold voltages from the two branches of the hysteresis curve.

Conflict of Interest: The authors declare no competing financial interest.

Acknowledgment. This work was supported by the Laboratory Directed Research and Development Program at Sandia National Laboratories, a multiprogram laboratory operated by Sandia Corporation, a Lockheed Martin Co., for the United States Department of Energy under Contract No. DEAC01-94-AL85000. A.A.K. acknowledges support from the Intelligence Community Postdoctoral Fellowship Program.

Supporting Information Available: Additional details and results for the TGA, MS TPD, and Raman experiments. This material is available free of charge *via* the Internet at http://pubs.acs.org.

REFERENCES AND NOTES

1. Franklin, A. D.; Luisier, M.; Han, S.-J.; Tulevski, G.; Breslin, C. M.; Gignac, L.; Lundstrom, M. S.; Haensch, W. Sub-10 nm Carbon Nanotube Transistor. *Nano Lett.* **2012**, *12*, 758–762.
2. Cao, Q.; Rogers, J. A. Ultrathin Films of Single-Walled Carbon Nanotubes for Electronics and Sensors: A Review of Fundamental and Applied Aspects. *Adv. Mater.* **2009**, *21*, 29–53.
3. Avouris, P.; Martel, R. Progress in Carbon Canotube Electronics and Photonics. *MRS Bull.* **2010**, *35*, 306–313.
4. Kauffman, D. R.; Star, A. Carbon Nanotube Gas and Vapor Sensors. *Angew. Chem., Int. Ed.* **2008**, *47*, 6550–6570.
5. Khalap, V. R.; Sheps, T.; Kane, A. A.; Collins, P. G. Hydrogen Sensing and Sensitivity of Palladium-Decorated Single-Walled Carbon Nanotubes with Defects. *Nano Lett.* **2010**, *10*, 896–901.
6. Arnold, M. S.; Green, A. A.; Hulvat, J. F.; Stupp, S. I.; Hersam, M. C. Sorting Carbon Nanotubes by Electronic Structure Using Density Differentiation. *Nat. Nanotechnol.* **2006**, *1*, 60–65.
7. Wu, J.; Xie, L.; Hong, G.; Lim, H. E.; Thendie, B.; Miyata, Y.; Shinohara, H.; Dai, H. Short Channel Field-Effect Transistors from Highly Enriched Semiconducting Carbon Nanotubes. *Nano Res.* **2012**, *5*, 388–394.
8. Park, S.; Lee, H. W.; Wang, H.; Selvarasah, S.; Dokmeci, M. R.; Park, Y. J.; Cha, S. N.; Kim, J. M.; Bao, Z. Highly Effective Separation of Semiconducting Carbon Nanotubes Verified *via* Short-Channel Devices Fabricated Using Dip-Pen Nanolithography. *ACS Nano* **2012**, *6*, 2487–2496.
9. Cao, Q.; Han, S.-J.; Tulevski, G. S.; Franklin, A. D.; Haensch, W. Evaluation of Field-Effect Mobility and Contact Resistance of Transistors That Use Solution-Processed Single-Walled Carbon Nanotubes. *ACS Nano* **2012**, *6*, 6471–6477.
10. Choi, S.-J.; Bennett, P.; Takei, K.; Wang, C.; Lo, C. C.; Javey, A.; Bokor, J. Short-Channel Transistors Constructed with Solution-Processed Carbon Nanotubes. *ACS Nano* **2012**, *7*, 798–803.
11. Islam, M. R.; Kormondy, K. J.; Silbar, E.; Khondaker, S. I. A General Approach for High Yield Fabrication of CMOS-Compatible All-Semiconducting Carbon Nanotube Field Effect Transistors. *Nanotechnology* **2012**, *23*, 125201.
12. Kim, W.-J.; Lee, C. Y.; O'Brien, K. P.; Plombon, J. J.; Blackwell, J. M.; Strano, M. S. Connecting Single Molecule Electrical Measurements to Ensemble Spectroscopic Properties for Quantification of Single-Walled Carbon Nanotube Separation. *J. Am. Chem. Soc.* **2009**, *131*, 3128–3129.
13. Stokes, P.; Khondaker, S. I. High Quality Solution Processed Carbon Nanotube Transistors Assembled by Dielectrophoresis. *Appl. Phys. Lett.* **2010**, *96*, 083110.
14. Kormondy, K. J.; Stokes, P.; Khondaker, S. I. High Yield Assembly and Electron Transport Investigation of Semiconducting-Rich Local-Gated Single-Walled Carbon Nanotube Field Effect Transistors. *Nanotechnology* **2011**, *22*, 415201.

15. Zhang, Z.-B.; Cardenas, J.; Campbell, E. E. B.; Zhang, S. L. Reversible Surface Functionalization of Carbon Nanotubes for Fabrication of Field-Effect Transistors. *App. Phys. Lett.* **2005**, *87*, 083110.
16. Geng, H.-Z.; Kim, K. K.; So, K. P.; Lee, Y. S.; Chang, Y.; Lee, Y. H. Effect of Acid Treatment on Carbon Nanotube-Based Flexible Transparent Conducting Films. *J. Am. Chem. Soc.* **2007**, *129*, 7758–7759.
17. Hilmer, A. J.; McNicholas, T. P.; Lin, S.; Zhang, J.; Wang, Q. H.; Mendenhall, J. D.; Song, C.; Heller, D. A.; Barone, P. W.; Blankschtein, D.; *et al.* Role of Adsorbed Surfactant in the Reaction of Aryl Diazonium Salts with Single-Walled Carbon Nanotubes. *Langmuir* **2012**, *28*, 1309–1321.
18. Usrey, M. L.; Lippmann, E. S.; Strano, M. S. Evidence for a Two-Step Mechanism in Electronically Selective Single-Walled Carbon Nanotube Reactions. *J. Am. Chem. Soc.* **2005**, *127*, 16129–16135.
19. Siitonen, A. J.; Tsyboulski, D. A.; Bachilo, S. M.; Weisman, R. B. Surfactant-Dependent Exciton Mobility in Single-Walled Carbon Nanotubes Studied by Single-Molecule Reactions. *Nano Lett.* **2010**, *10*, 1595–1599.
20. Geng, H.-Z.; Lee, D. S.; Kim, K. K.; Han, G. H.; Park, H. K.; Lee, Y. H. Absorption Spectroscopy of Surfactant-Dispersed Carbon Nanotube Film: Modulation of Electronic Structures. *Chem. Phy. Lett.* **2008**, *455*, 275–278.
21. Kiowski, O.; Lebedkin, S.; Hennrich, F.; Kappes, M. M. Single-Walled Carbon Nanotubes Show Stable Emission and Simple Photoluminescence Spectra with Weak Excitation Sidebands at Cryogenic Temperatures. *Phys. Rev. B* **2007**, *76*, 075422-1–075422-8.
22. Li, X.; Zhang, L.; Wang, X.; Shimoyama, I.; Sun, X.; Seo, W.-S.; Dai, H. Langmuir–Blodgett Assembly of Densely Aligned Single-Walled Carbon Nanotubes from Bulk Materials. *J. Am. Chem. Soc.* **2007**, *129*, 4890–4891.
23. Duque, J. G.; Hamilton, C. E.; Gupta, G.; Crooker, S. A.; Crochet, J. J.; Mohite, A.; Htoon, H.; DeFriend Obrey, K. A.; Dattelbaum, A. M.; Doorn, S. K. Fluorescent Single-Walled Carbon Nanotube Aerogels in Surfactant-Free Environments. *ACS Nano* **2011**, *5*, 6686–6694.
24. Lee, H. W.; Yoon, Y.; Park, S.; Oh, J. H.; Hong, S.; Liyanage, L. S.; Wang, H.; Marishita, S.; Patil, N.; Park, Y. J.; *et al.* Selective Dispersion of High Purity Semiconducting Single-Walled Carbon Nanotubes with Regioregular Poly(3-alkylthiophene)s. *Nat. Commun.* **2011**, *2*, 541.
25. Lu, K. L.; Lago, R. M.; Chen, Y. K.; Green, M. L. H.; Harris, P. J. F.; Tsang, S. C. Mechanical Damage of Carbon Nanotubes by Ultrasound. *Carbon* **1996**, *34*, 814–816.
26. Vosgueritchian, M.; LeMieux, M. C.; Dodge, D.; Bao, Z. Effect of Surface Chemistry on Electronic Properties of Carbon Nanotube Network Thin Film Transistors. *ACS Nano* **2010**, *4*, 6137–6145.
27. Hou, P. X.; Liu, C.; Cheng, H. M. Purification of Carbon Nanotubes. *Carbon* **2008**, *46*, 2003–2025.
28. Ng, M. H. A.; Hartadi, L. T.; Tan, H.; Poa, C. H. P. Efficient Coating of Transparent and Conductive Carbon Nanotube Thin Films on Plastic Substrates. *Nanotechnology* **2008**, *19*, 205703.
29. Tenent, R. C.; Barnes, T. M.; Bergeson, J. D.; Ferguson, A. J.; To, B.; Gedvilas, L. M.; Heben, M. J.; Blackburn, J. L. Ultrasmooth, Large-Area, High-Uniformity, Conductive Transparent Single-Walled-Carbon-Nanotube Films for Photovoltaics Produced by Ultrasonic Spraying. *Adv. Mater.* **2009**, *21*, 3210–3216.
30. Zhang, Q. H.; Zhang, Q.; Vichchulada, P.; Shivareddy, S. B.; Lay, M. D. Reducing Electrical Resistance in Single-Walled Carbon Nanotube Networks: Effect of the Location of Metal Contacts and Low-Temperature Annealing. *J. Mater. Sci.* **2012**, *47*, 3233–3240.
31. Joo, M.; Lee, M. Laser Treatment of Solution-Deposited Carbon Nanotube Thin Films for Improved Conductivity and Transparency. *Nanotechnology* **2011**, *22*, 265709.
32. Tan, Y. Q.; Resasco, D. E. Dispersion of Single-Walled Carbon Nanotubes of Narrow Diameter Distribution. *J. Phys. Chem. B* **2005**, *109*, 14454–14460.
33. Youssry, M.; Coppola, L.; Furia, E.; Oliviero, C.; Nicotera, I. A New Physicochemical Characterization of Sodium Taurodeoxycholate/Water System. *Phys. Chem. Chem. Phys.* **2008**, *10*, 6880–6889.
34. Moon, J. M.; An, K. H.; Lee, Y. H.; Park, Y. S.; Bae, D. J.; Park, G.-S. High-Yield Purification Process of Singlewalled Carbon Nanotubes. *J. Phys. Chem. B* **2001**, *105*, 5677–5681.
35. Chiang, I. W.; Brinson, B. E.; Smalley, R. E.; Margrave, J. L.; Hauge, R. H. Purification and Characterization of Single-Wall Carbon Nanotubes. *J. Phys. Chem. B* **2001**, *105*, 1157–1161.
36. Romanos, G. E.; Likodimos, V.; Marques, R. R. N.; Steriotis, T. A.; Papageorgiou, S. K.; Faria, J. L.; Figueiredo, J. L.; Silva, A. M. T.; Falaras, P. Controlling and Quantifying Oxygen Functionalities on Hydrothermally and Thermally Treated Single-Wall Carbon Nanotubes. *J. Phys. Chem. C* **2011**, *115*, 8534–8546.
37. Collins, P. G. Defects and Disorder in Carbon Nanotubes. In *Oxford Handbook of Nanoscience and Technology: Frontiers and Advances*; Narlikar, A.V., Fu, Y.Y., Eds.; Oxford University Press: Oxford UK, 2010.
38. Ford, A. C.; Shaughnessy, M.; Wong, B. M.; Kane, A. A.; Kuznetsov, O. V.; Krafcik, K. L.; Billups, W. E.; Hauge, R. H.; Léonard, F. Physical Removal of Metallic Carbon Nanotubes from Nanotube Network Devices Using a Thermal and Fluidic Process. *Nanotechnology* **2013**, *24*, 105202.
39. Saito, R.; Fantini, C.; Jiang, J. Excitonic States and Resonance Raman Spectroscopy of Single-Wall Carbon Nanotubes. In *Carbon Nanotubes: Advanced Topics in the Synthesis, Structure, Properties, and Applications*; Jorio, A., Dresselhaus, G., Dresselhaus, M. S., Eds.; Springer-Verlag: Berlin, 2008; pp 251–286.
40. Nguyen, K. T.; Gaur, A.; Shim, M. Fano Lineshape and Phonon Softening in Single Isolated Metallic Carbon Nanotubes. *Phys. Rev. Lett.* **2007**, *98*, 145504.
41. Kavan, L.; Kalbac, M.; Zukalova, M.; Dunsch, L. Electrochemical Doping of Chirality-Resolved Carbon Nanotubes. *J. Phys. Chem. B* **2005**, *109*, 19613–19619.
42. Kalbac, M.; Hsieh, Y.-P.; Farhat, H.; Kavan, L.; Hofmann, M.; Kong, J.; Dresselhaus, M. S. Defects in Individual Semiconducting Single Wall Carbon Nanotubes: Raman Spectroscopic and *In Situ* Raman Spectroelectrochemical Study. *Nano Lett.* **2011**, *11*, 4619–4626.
43. Li-Pook-Than, A.; Lefebvre, J.; Finnie, P. Type- and Species-Selective Air Etching of Single-Walled Carbon Nanotubes Tracked with *In Situ* Raman Spectroscopy. *ACS Nano* **2013**, *7*, 6507–6521.
44. Abdula, D.; Nguyen, K. T.; Shim, M. Raman Spectral Evolution in Individual Metallic Single-Walled Carbon Nanotubes upon Covalent Sidewall Functionalization. *J. Phys. Chem. C* **2007**, *111*, 17755–17760.
45. Dresselhaus, M. S.; Jorio, A.; Hofmann, M.; Dresselhaus, G.; Saito, R. Perspectives on Carbon Nanotubes and Graphene Raman Spectroscopy. *Nano Lett.* **2010**, *10*, 751–758.
46. Zhou, X.; Zifer, T.; Wong, B. M.; Krafcik, K. L.; Léonard, F.; Vance, A. L. Color Detection Using Chromophore–Nanotube Hybrid Devices. *Nano Lett.* **2009**, *9*, 1028–1033.